Honeycomb-Like Organized TiO_2 Photoanodes with Dual Pores for Solid-State Dye-Sensitized Solar Cells

*Sung Hoon Ahn, Won Seok Chi, Dong Jun Kim, Sung Yeon Heo, and Jong Hak Kim**

A solid-state dye-sensitized solar cell (ssDSSC) with 7.4% efficiency at 100 mW/cm^2 is reported. This efficiency is one of the highest observed for N719 dye. High performance is achieved via a honeycomb-like, organized mesoporous TiO_2 photoanode with dual pores, high porosity, good interconnectivity, and excellent light scattering properties. The TiO_2 photoanodes are prepared without any $TiCl_4$ treatment via a one-step, direct self-assembly of hydrophilically preformed TiO_2 nanocrystals and poly(vinyl chloride)-*g*-poly(oxyethylene methacrylate) (PVC-*g*-POEM) graft copolymer as a titania source and a structure-directing agent, respectively. Upon controlling the secondary forces between the polymer/TiO_2 hybrid and the solvent by varying the amounts of HCl/H_2O mixture or toluene, honeycomb-like structures are generated to improve light scattering properties. Such multifunctional nanostructures with dual pores provide good pore-filling of solid polymer electrolyte with large volume, enhanced light harvesting and reduced charge recombination, as confirmed by reflectance spectroscopy, incident photon-to-electron conversion efficiency (IPCE), and electrochemical impedance spectroscopy (EIS) analysis.

1. Introduction

Since the Gratzel group introduced dye-sensitized solar cells (DSSCs) in 1991,[1] the material has received tremendous interest due to its high efficiency, low fabrication cost and ease of fabrication. Despite the high energy conversion efficiency (≈11%) of DSSCs with a I^-/I_3^- liquid electrolyte, solid-state DSSCs (ssDSSCs) have recently received much attention due to the need for long-term stability, flexible design and lightweight cells.[2–8] Several approaches have been reported for ssDSSCs based on a hole conducting polymer[9–14] or a solid polymer electrolyte.[15–17] However, most of the efficiencies reported for ssDSSCs are less than 7%, which are below the efficiencies of their counterparts using a liquid electrolyte.[2–17] Recently, a high efficiency of 8.5% has been achieved by the Kanatzidis group using $CsSnI_3$ perovskite as a hole conductor.[18] The independent Snaith and Park groups also reported a high efficiency of 10.9% and 9.7%, respectively, using $(CH_3NH_3)PbX$ (X = Cl, I) perovskite and spiro-MeOTAD as a light harvester and a hole conductor, respectively.[19] However, these high efficiencies were achieved through developing a novel hole conductor or sensitizer, implying that cell performance would be further improved if it is combined with a more effective organized TiO_2 photoanode.

One of the key considerations in fabricating ssDSSCs is to enable deep infiltration of large volume solid electrolytes into the TiO_2 photoanode, which largely depends on the pore structure and morphology of TiO_2. In particular, the energy conversion efficiency of DSSCs with well-organized TiO_2 photoanodes is much greater than those with traditional randomly structured photoanodes due to their high porosity and good interconnectivity.[20] A colloidal crystal template and holographic lithography have been introduced to produce well-organized TiO_2 photoanodes,[21,22] but their surface areas were not high enough to load a large amount of dye molecules. Block copolymer-templated synthetic strategies are also effective for preparing well-organized TiO_2 photoanodes.[9–11] However, the synthesis of block copolymers is sensitive to impurities such as H_2O and O_2, requiring synthetic expertise and thus high cost. Use of a commercially available block copolymer, e.g., Pluronic P123, often leads to TiO_2 pore sizes smaller than 10 nm due to the low molecular weight of the copolymer, which hinders thorough infiltration of solid electrolytes and impedes the complete crystallization while maintaining structural integrity.[9] Our group recently reported a high efficiency (7.1%) ssDSSC based on micron-thick, organized mesoporous TiO_2 photoanodes prepared through a direct self-assembly of a graft copolymer, i.e., poly(vinyl chloride)-*g*-poly(oxyethylene methacrylate) (PVC-*g*-POEM), and preformed TiO_2 nanocrystals with an elongated spherical shape.[16a] Although these photoanodes were effective for solid polymer electrolytes, light scattering properties were limited due to high transparency.

Light scattering properties can be improved by incorporation of scattering particles, but this often reduces the dye loading capacity of the photoanode. The double layer structure consisting of a nanocrystalline main layer and a large size scattering layer also results in an increase in photoanode thickness, leading to electron recombination. Submicrometer-sized

S. H. Ahn, W. S. Chi, D. J. Kim, S. Y. Heo,
Prof. J. H. Kim
Department of Chemical and Biomolecular Engineering
Yonsei University
262 Seongsanno Seodaemun-gu
Seoul 120-749, South Korea
E-mail: jonghak@yonsei.ac.kr

DOI: 10.1002/adfm.201203851

mesoporous TiO_2 beads are considered to be materials with dual functions of high dye loading and efficient scattering, but $TiCl_4$ treatment is often required to improve interconnectivity between the beads.[23–25] Another approach to enhance light harvesting efficiency is to incorporate a photonic crystal layer such as a Bragg reflector into the photoanode structure.[26,27] In particular, the hierarchically structured photoanodes may improve the cell efficiencies by imparting extra functions, such as providing a large surface area, generating light scattering, enhancing electron transport and facilitating electrolyte diffusion.[28] However, small pore size of TiO_2 photoanodes could hinder the deep infiltration of solid electrolyte into the nanopores.

In this work, we report the ssDSSC with 7.4% efficiency at 100 mW/cm^2 is reported, one of the highest observed for N719 dye, based on honeycomb-like, organized mesoporous TiO_2 photoanode with dual pores, high porosity, good interconnectivity and excellent light scattering properties. The TiO_2 photoanode is prepared via a sol-gel process using a PVC-*g*-POEM graft copolymer as a structure directing agent. A graft copolymer is more attractive than a block copolymer due to its low cost and the ease with which it can be synthesized. The various morphologies of TiO_2 photoanode are obtained by changing the interactions between the polymer/TiO_2 hybrid and the solvent. The ssDSSCs are fabricated using a solid-state polymerized ionic liquid (PIL) and their performance is characterized using current–voltage (*J*–*V*) curves and incident photon to current conversion efficiency (IPCE) spectra. Light harvesting and charge recombination kinetics are characterized by reflectance spectroscopy, IPCE, and electrochemical impedance spectroscopy (EIS) analysis.

2. Results and Discussion

A facile, effective method is developed to improve the light harvesting properties of TiO_2 photoanodes without disrupting organized structures through a control of specific interactions between the polymer/TiO_2 hybrids and the solvent. The organized structure is an excellent candidate as a photoelectrode for ssDSSCs because it can allow for facile penetration of the large molecular weight polymer into the TiO_2 nanopores. The preparation involves a one-step, direct self-assembly of the PVC-*g*-POEM graft copolymer and the hydrophilically preformed TiO_2 nanocrystals without any additives, as illustrated in **Figure 1**. The PVC-*g*-POEM graft copolymer plays a pivotal role as a structure directing agent due to well-defined, microphase-separated structure, resulting from the flexible, hydrophilic properties of rubbery POEM chains (glass transition temperature, T_g = –58 °C) and the rigid, hydrophobic properties of glassy PVC chains (T_g = 70 °C).[16c] Also, the amorphous nature and high molecular weight (weight-average molecular weight, $M_w = 1.1 \times 10^5$ g/mol, polydispersity index, PDI = 2.2) of PVC-*g*-POEM can generate large pores, which faciliates deep infiltration of solid electrolytes and promotes the complete titania crystallization while maintaining structural integrity. The hydrophilicity of preformed TiO_2 arises from the surface-modification with benzyl alcohol, which plays a role as a capping agent for inorganic nanocrystals. Benzyl alcohol provides selective, preferential interaction with the hydrophilic POEM domains of the PVC-*g*-POEM graft copolymer. Thus, the amphiphilic PVC-*g*-POEM graft copolymer worked as a structure-directing agent not only on a mesoscopic scale, forming self-assembly of micelles, but also in macroscopic crystal growth of TiO_2.

Figure 2 shows field emission scanning electron microscopy (FE-SEM) images of TiO_2 films prepared by changing the amounts of HCl/H_2O mixture or toluene. All the TiO_2 films exhibited organized mesoporous structures with a high porosity, large pores and good interconnectivity, but the size of the honeycomb-like structures varied. Well-organized, worm-like structures with large pores, high porosity, and good interconnectivity without large grain boundaries were obtained for the organized mesoporous (OM) TiO_2 film (Figure 2a) prepared using a good solvent mixture consisting of the large amounts of tetrahydrofuran (THF) and small amounts of toluene:(HCl/H_2O) mixture. The solubility parameter (δ) is a good indicator for polymer-solvent interactions. Since the δ of THF closely matches those of PVC and POEM, THF is a good solvent for both chains; THF = 9.5, PVC = 9.6 and POEM = 10.8 cal$^{1/2}$ cm$^{-3/2}$.[29] In a good solvent, the secondary forces between polymer segments and solvent molecules are strong and thus both PVC and POEM chains are highly stretched in a spread-out conformation.

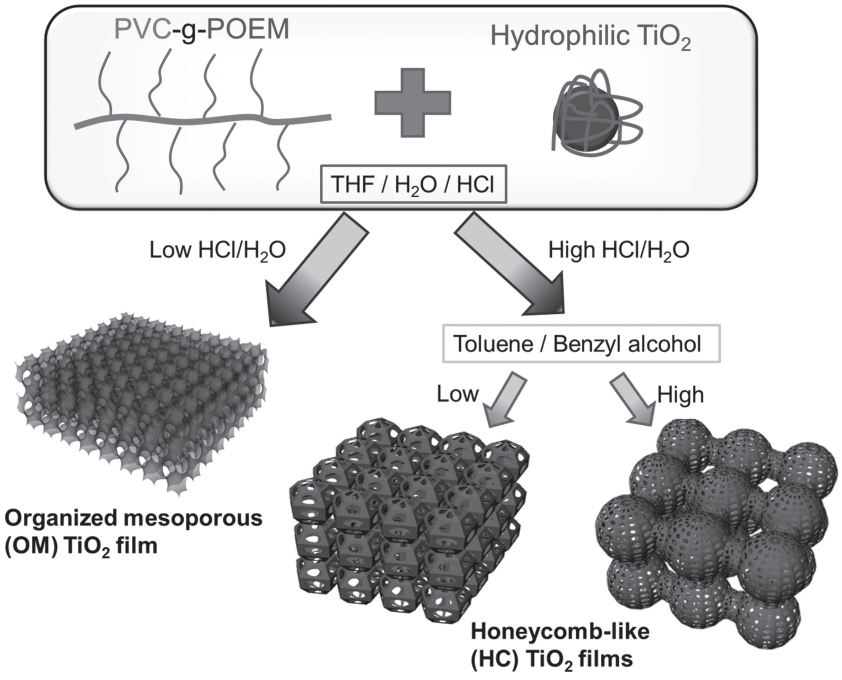

Figure 1. Schematic of the preparation of OM and HC series TiO_2 films using PVC-g-POEM graft copolymer and hydrophilically preformed TiO_2 nanocrystals.

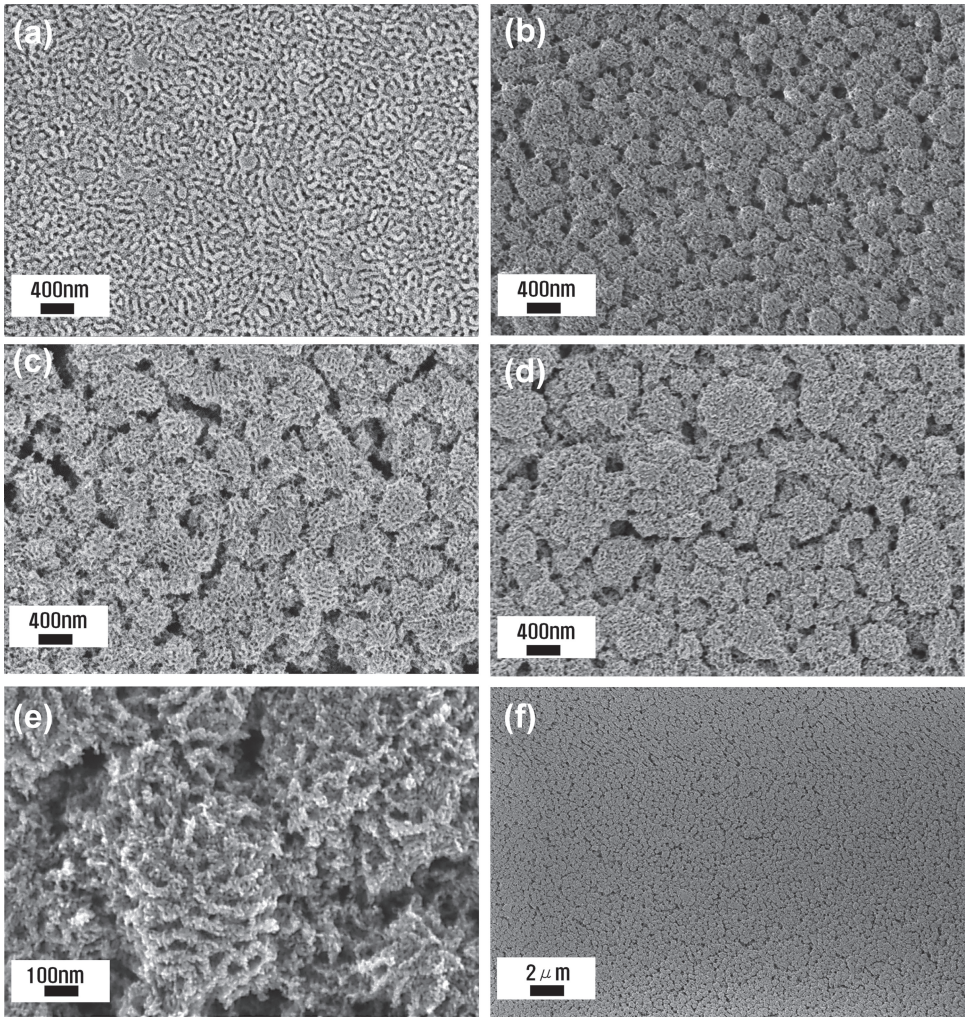

Figure 2. FE-SEM surface images of TiO_2 films: a) OM, b) HC1, c) HC2, d) HC3, e) high magnification of HC2, and f) low magnification of HC2.

The bright regions in Figure 2 represent the TiO_2 matrix, whereas the dark regions show pores. Such an organized structure aids in facile penetration of the solid polymer electrolyte with large molecular volume into the nanopores. This structure arose from the function of the preformed TiO_2 nanocrystals, which act as building blocks and have selective interactions with the hydrophilic POEM side chains of the graft copolymer template. Upon evaporation of the solvent and calcination at 450 °C, the polymer/TiO_2 hybrid materials phase-separate into nanometer-sized domains, where the TiO_2 sol resides in the hydrophilic POEM regions to form a matrix around the pore-forming hydrophobic PVC regions.

Honeycomb-like (HC) structures with meso/macroscopic dual pores were generated by controlling the polymer-solvent interactions, as shown in Figure 2b where the amount of HCl/H_2O mixture varied from 0.1 to 0.3 mL. The HCl/H_2O mixture (δ of water = 23.5 $cal^{1/2}$ $cm^{-3/2}$) is a poor solvent for the PVC chains but a relatively good solvent for POEM/TiO_2 hybrids.[30] Thus, the interfacial energy between the POEM/TiO_2 hybrids and the solvent would be reduced with HCl/H_2O content, leading to increased volume expansion of the POEM/TiO_2 domains, which produced HC structures with meso/macroscopic pores. The size of the HC structures continuously increased with increasing amounts of toluene, as shown in Figure 2b–d and Figure S1 (Supporting Information). Because toluene, which is a water-immiscible nonpolar liquid and mono-substituted benzene derivative (δ of toluene = 8.9 $cal^{1/2}$ $cm^{-3/2}$)[30] is a poor solvent for PVC chains as well as POEM/TiO_2 hybrids, the interaction between the solvent and the PVC-*g*-POEM/TiO_2 hybrids would be reduced, resulting in a mesoscopic self-aggregated structure.

A magnified surface image (Figure 2e) revealed that the HC film contains bimodal pores consisting of small mesopores (10–40 nm) and large macropores (100–200 nm), which are effective in providing a large surface area as well as allowing for facile pore infiltration of solid polymer electrolytes. The organized structure was maintained in the HC films, indicating that the addition of poor solvents such as water and toluene did not perturb the mesoporosity or interconnectivity. A crack-free surface with good homogeneity and uniformity over large areas was obtained, as illustrated by a low magnification FE-SEM image, shown in Figure 2f. The HC4 film prepared with a large amount (25 mL) of toluene also showed excellent light scattering properties (as shown in Figure S1,

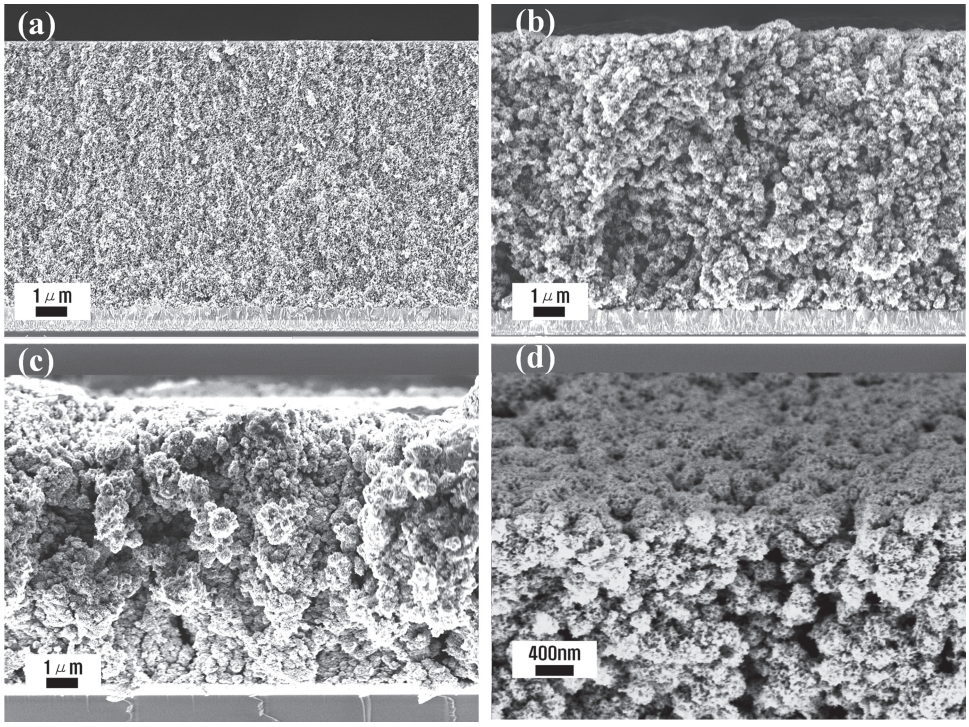

Figure 3. Cross-sectional FE-SEM images of TiO_2 films: a) OM, b) HC-1, c) HC-2, and d) tilted image with an angle of 15° of HC-1.

Supporting Information) but was not used in this study due to the poor mechanical stability of the film. Cross-sectional FE-SEM images of TiO_2 films (**Figure 3**) show the formation of a three-dimensional structure with high porosity, large pores, good interconnectivity and excellent light-scattering properties. Crack-free, approximately 8.5-μm-thick TiO_2 films on SnO_2/F-layered (FTO) glass were prepared via a one-step doctor blading technique, indicating large-scale processability. This was possible because the hydrophilically preformed TiO_2 nanocrystals possessed lower volume contraction upon calcination at 450 °C and played an important role as building blocks through preferential, strong interaction with the POEM domains of PVC-*g*-POEM graft copolymer.

The efficiency of DSSCs largely depends on the amount of dye loading, which is related, in turn, to the pore structure, connectivity, surface area and porosity of the TiO_2 films. The surface areas and pore size distributions of the TiO_2 films were determined by nitrogen adsorption-desorption and analyzed using the Barrett–Joyner–Halenda (BJH) method (**Figure 4**, **Table 1**). Macropores larger than 100 nm shown in the FE-SEM images were unobservable due to the difference in scale ranges. In order to achieve better interconnectivity, the reaction time for preformed TiO_2 in this study was increased to 15 h, which is longer than the previous experiment.[16a] This resulted in an increase in particle size and the amount of capping organics, i.e., benzyl alcohol, at the particle surface, leading to better interconnectivity and higher electron transport. It is well known that nanoparticle size shows a trade-off behavior between surface area and electron transport.[31] The pore size distribution curves in Figure 4b show that a main peak maximum was shifted to a larger pore size position as the honeycomb size increased. Overall, the surface area and the dye loading of the OM film were the highest, while the HC-2 and HC-3 films were not significantly different from each other.

Since DSSC efficiency is also strongly dependent on the light scattering ability of the electrode, the UV-visible reflectance spectra of TiO_2 photoanodes were measured, as shown in **Figure 5**a. The reflectance of the HC films was always much greater than that of OM, indicating effective light scattering ability of HC a few hundred nanometers in size. The reflectance ability of HC films continuously increased with the size of the HC. Overall, the TiO_2 photoanodes derived from large-sized HC showed higher reflectance than those from small-sized ones. A higher photonic reflectance value close to 60% was obtained for HC3 in the range of 400–800 nm, which provides a basis for the effective use of long wavelength photonic energy. Thus, HC films could extend the photoresponse of the photoanode well into the visible spectrum, resulting in an enhancement of light utilization efficiency.

Light scattering properties were also evaluated by measuring the IPCE spectra in the higher wavelength regions. The IPCE curves of ssDSSCs fabricated with TiO_2 photoanodes are shown in Figure 5b as a function of illumination wavelength. Poly((1-(4-ethenylphenyl)methyl)-3-butyl-imidazolium iodide) (PEBII)[5] was synthesized via free radical polymerization as a polymerized ionic liquid and utilized as a solid electrolyte for I_2-free ssDSSCs without using any additives. The synthesized PEBII showed high mobility and ionic conductivity (2.0×10^{-4} S/cm at 25 °C) due to facile ion transportation through the well-organized structure with π-π stacking interaction and low T_g (≈ −4 °C). The ssDSSCs with HC photoanodes exhibited higher IPCE values than that with an OM photoanode in the ranges of 450–750 nm, indicating greater light harvesting effect in the former. Normalized IPCE curves in Figure S2 (Supporting

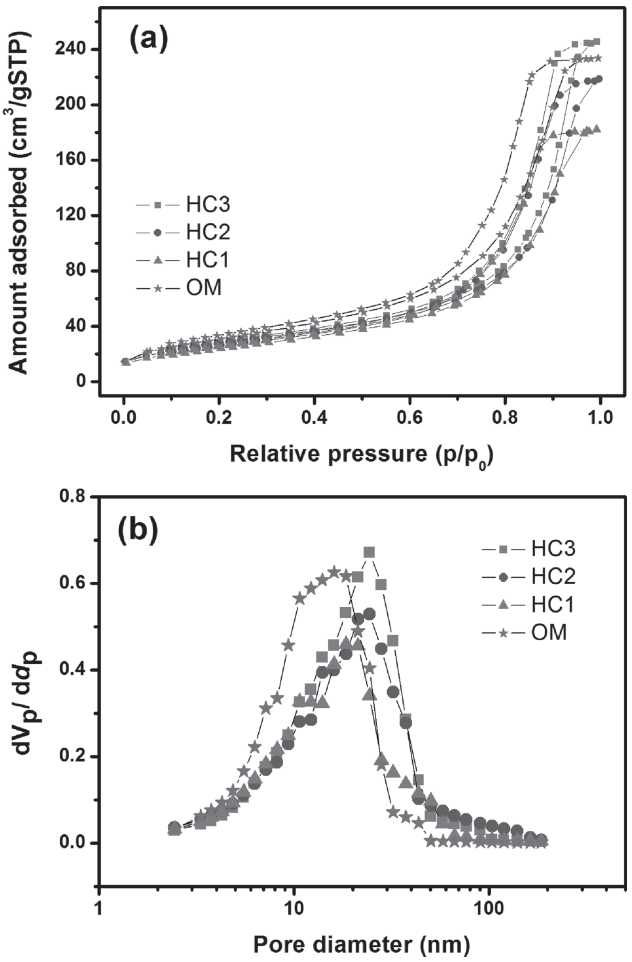

Figure 4. a) N_2 adsorption-desorption curves of mesoporous TiO_2 films and b) pore size distributions of TiO_2 films determined using the BJH method.

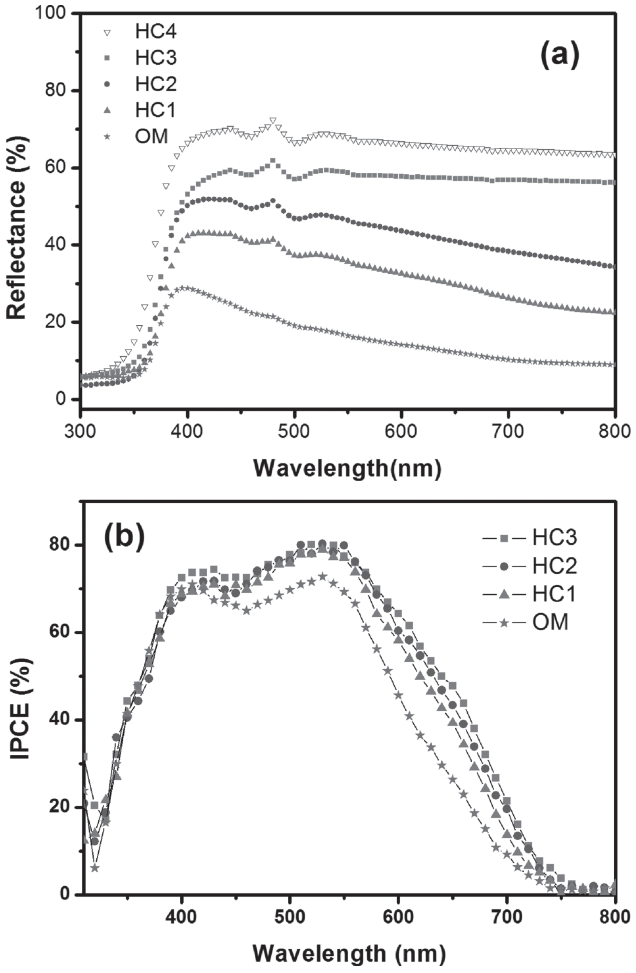

Figure 5. a) Reflectance spectra of TiO_2 films deposited on FTO glasses and b) IPCE curves of the ssDSSC fabricated with 8.5-μm thick TiO_2 electrode and solid PEBII electrolyte at 100 mW/cm^2.

Information) clearly show the enhanced quantum efficiency of HC photoanodes due to the strong light scattering effect over the visible range, which is consistent with the above reflectance results.

Table 1. Surface area, dye loading and photovoltaic properties of ssDSSCs fabricated with an 8.5-μm-thick TiO_2 photoanode and a solid PEBII[a)] electrolyte at 100 mW/cm^2 (AM 1.5).

Photoanode[b)]	Surface area [m^2/g]	Dye loading [nmol/cm^2]	V_{oc} [V]	J_{sc} [mA/cm^2]	FF	η [%]
OM	116.0	102.1	0.75	13.9	0.59	6.1
HC-1	89.7	91.4	0.75	15.9	0.60	7.1
HC-2	97.4	93.3	0.74	17.2	0.58	7.4
HC-3	99.8	94.6	0.73	18.0	0.54	7.0
Dyesol	–	83.2	0.73	11.0	0.50	4.0

[a)]EBII: poly(1-((4 ethenylphenyl)methyl)-3-butyl-imidazolium iodide)); [b)]OM: organized mesoporous TiO_2 film prepared with toluene:(HCl/H_2O) = 10:0.1 vol ratio; HC-1: honeycomb-like TiO_2 film prepared with toluene:(HCl/H_2O) = 10:0.3; HC-2: toluene:(HCl/H_2O) = 15:0.3; HC-3: toluene:(HCl/H_2O) = 20:0.3. Dyesol: commercially available Dyesol paste (18NR-T).

The current density-voltage (J–V) curves of ssDSSCs fabricated with the 8.5-μm-thick TiO_2 films and PEBII as a photoanode and a solid electrolyte, respectively, were measured as shown in **Figure 6**a. Cell performance including open-circuit photovoltage (V_{oc}), short-circuit current density (J_{sc}), fill factor (FF) and an energy conversion efficiency (η) are summarized in Table 1. The conversion efficiencies of HC series and OM cells without any $TiCl_4$ treatment were always greater than that of less-organized TiO_2 cell (4.0%) prepared using the commercially available Dyesol paste 18NR-T. It indicates the importance of an organized structure of photoanode in ssDSSCs, where deep penetration of solid electrolyte is most important and thus the effect of organized structure is obvious. The higher efficiencies of HC series and OM cells are due to a larger surface area and well-developed organized mesoporous structure, resulting in greater dye adsorption, deep penetration of solid electrolyte and enhanced electron transport. In particular, the conversion efficiency of the HC-2 cell reached 7.4% at 100 mW/cm^2, which is one of the highest values observed for N719 based ssDSSCs[9]–[17] and approximately 1.7-fold greater than that of commercially available TiO_2. The obtained cell efficiency was

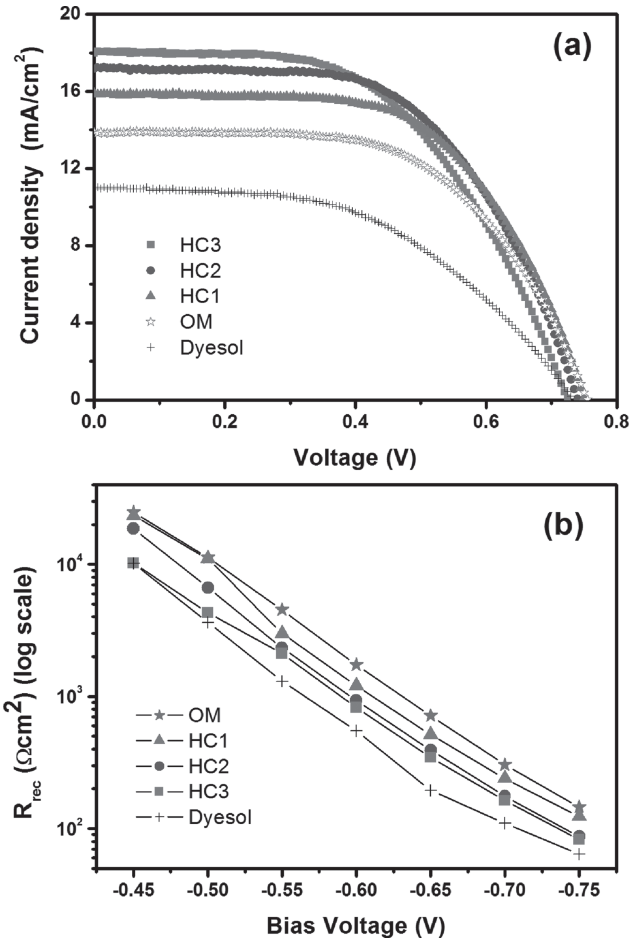

Figure 6. a) *J–V* curves of the ssDSSC fabricated with 8.5-μm thick TiO_2 electrode and solid PEBII electrolyte at 100 mW/cm^2. b) Recombination resistances (R_{rec}) determined by EIS experiment under dark conditions.

maintained for 200 h at room temperature. Also, the conversion efficiency of the HC-2 cell is approximately a 20% enhancement over that of the OM cell (6.1%). This improvement mostly resulted from the enhancement of the J_{sc} value, as the V_{oc} and FF values were not significantly changed. Because the surface area and dye loading of HC-2 film are lower than those of OM film, the greater J_{sc} value of the former would be attributed to excellent light scattering ability, resulting from the well-organized, interconnected HC structure with dual pores, as confirmed by UV-visible reflectance spectroscopy and IPCE results in Figure 5.

Despite a higher J_{sc} value for the HC-3 cell, its V_{oc} and FF values were reduced, resulting in lower efficiency than that of the HC-2 cell, which may be related to electron transport properties. Thus, the electron transport and charge recombination kinetics of ssDSSCs were investigated using EIS in the dark, as shown in Figure S3 (Supporting Information). The Nyquist plot obtained for each cell shows three semicircles that reflect i) the charge transfer resistance at the counter electrode in the kHz region, ii) the Nernst-type impedance due to electron transport across the nanocrystalline titania layer and their recapture by tri-iodide in the Hz region and iii) finally the so-called finite-Warburg impedance relative to the tri-iodide mass transport in the mHz region. All spectra recorded were simulated and plotted using Z plot software with an equivalent circuit that depicts a general transmission line electrical model established originally to describe the macroscopic homogeneous porous electrode model. The logarithm of the recombination resistances (R_{rec}) derived from the impedance data are plotted in Figure 6b) as a function of bias voltage. As shown, the logarithmic plots present the almost linear dependence of recombination resistances as a function of bias voltage for the all the photoanodes. The electron recombination resistances of HC series and OM cells were always larger than that of less-organized TiO_2 cell prepared using the commercially available paste (Dyesol, 18NR-T). It indicates the importance of an organized structure for electron transport, which is attributed to the large pore size and good interconnectivity resulting in the improved interfacial contact of the electrode/electrolyte. The HC3 photoanode with a larger HC size was less effective in electron transport than the other photoanodes resulting from decreased interconnectivity between TiO_2 but better than less-organized TiO_2 cell. This is consistent with the FE-SEM images and explains the lower efficiency of the HC3 cell compared to the HC-2 cell. Thus, there is a trade-off between light scattering properties and electron transport.

3. Conclusion

In summary, meso/macroscopic interconnected honeycomb-like nanostructured TiO_2 photoanodes with dual pores were prepared via careful control of hybrid sol/solvent interactions using direct assembly of the hydrophilically preformed TiO_2 nanocrystals and the amphiphilic PVC-g-POEM graft copolymer. The amphiphilic PVC-g-POEM graft copolymer worked as a structure-directing agent not only on a mesoscopic scale, forming self-assembly of micelles, but also in macroscopic crystal growth of TiO_2. A honeycomb-like structure was generated by increasing the amount of HCl/H_2O mixture, a poor solvent for the PVC main chains while its size increased with increasing amounts of toluene, which is a poor solvent for the POEM side chains as well as PVC chains. The efficiencies of HC series and OM cells were always greater than that of less-organized TiO_2 cell (4.0%) prepared using the commercially available paste (Dyesol, 18NR-T). In particular, the conversion efficiency of the HC-2 cell without any $TiCl_4$ treatment was the highest, 7.4% at 100 mW/cm^2, which is one of the highest values observed for ssDSSCs. The higher cell efficiency is attributed to the enhanced J_{sc} value resulting from the well-organized, interconnected HC structure with large pores, high porosity and excellent light scattering ability.

4. Experimental Section

Materials: Poly(vinyl chloride) (PVC, M_n = 55 000 g mol^{-1}), poly(oxyethylene methacrylate) (POEM, poly(ethylene glycol) methyl ether methacrylate, M_n = 475 g mol^{-1}), 1,1,4,7,10,10-hexamethyltriethylene tetramine (HMTETA, 99%), copper(I) chloride (CuCl, 99%), titanium(IV) isopropoxide (TTIP, 97%), hydrogen chloride solution (HCl, 37 wt%), chloroplatinic acid hexahydrate (H_2PtCl_6) were purchased

from Sigma-Aldrich. Tetrahydrofuran (THF), *N*-methyl pyrrolidone (NMP), methanol, 2-propanol, chloroform, acetonitrile, diethylether and ethyl acetate were purchased from J.T. Baker. Deionized water (>18 MΩ m) was obtained with a water purification system made by Millipore Corporation. Ruthenium dye (535-bisTBA, N719) was purchased from Solaronix, Switzerland. Fluorine-doped tin oxide (FTO) conducting glass substrate (TEC8, 8 ohms/sq, 2.3 mm thick) was purchased from Pilkington, France. All solvents and chemical reagents used in our experiments were obtained from commercial sources as guaranteed grade reagents and used without further purification.

Synthesis of the PVC-g-POEM Graft Copolymer Template: PVC-*g*-POEM graft copolymer was synthesized via atomic transfer radical polymerization (ATRP) process, according to the previously reported method.[16c] In brief, 6 g of PVC was dissolved in 50 mL of NMP by stirring at 90 °C for 4 h. After cooling the solution to room temperature, 15 g of POEM, 0.1 g of CuCl, and 0.23 mL of HMTETA were added to the solution. The green mixture was stirred until producing homogeneous solution, and was purged with nitrogen for 30 min. The reaction was carried out at 90 °C for 18 h. After polymerization, the resultant mixture was diluted with THF. After passing the solution through a column with activated Al_2O_3 to remove the catalyst, the solution was precipitated into methanol. The grafted copolymer was purified by dissolving in THF and re-precipitating into methanol three times. PVC-*g*-POEM graft copolymer with PVC:POEM = 1: 1.5 wt% ratio was obtained in a powder form and dried in a vacuum oven overnight at room temperature.

Synthesis of the Meso/Macroscopic Organized TiO_2 Photoanodes: Preformed TiO_2 nanocrystals were synthesized by slightly modifying a previously reported method.[16a] First, 1.5 mL of $TiCl_4$ was slowly added to 10,15, 20 or 25 mL of toluene and was stirred for a few seconds to produce a homogeneous solution. The solution was carefully added to 50 mL of benzyl alcohol and stirred for 30 min. This transparent, yellowish solution was heated in a convection oven at 70 °C for 15 h, after which white precipitates were obtained. The precipitated TiO_2 nanocrystals were isolated by centrifugation at 12 000 rpm for 30 min.

Then, 0.2 g of PVC-*g*-POEM graft copolymer was dissolved in 1.8 mL of tetrahydrofuran, and then 0.4 g of the preformed TiO_2 nanocrystals were added to the polymer solution. In order to induce self-assembly of the PVC-g-POEM/TiO_2 mixture, 0.1 mL of a HCl/H_2O mixture (37:63 wt. ratio) was added, followed by stirring overnight. The TiO_2 film prepared with a toluene:(HCl/H_2O) = 10:0.1 vol. ratio, was considered an organized mesoporous (OM) film. When 0.3 mL of a HCl/H_2O mixture was added to the polymer solution, honeycomb-like structures were observed. The HC-1, HC-2, HC-3 and HC-4 films were prepared with toluene:(HCl/H_2O) = 10:0.3, 15:0.3, 20:0.3 and 25:0.3 volume ratios, respectively. The viscous mixture was cast onto the FTO substrate using the doctor blade technique and was aged for 30 min at ambient conditions. In order to remove the polymer template and organic compounds, the TiO_2 photoanodes were calcined at 450 °C for 30 min.

Fabrication of the ssDSSCs: The ssDSSCs with an active area of 0.16 cm^2 were fabricated by drop-casting the polymer electrolyte solution onto the photoanode and covering with the counter electrode, following a previously reported procedure.[16] Transparent SnO_2/F-layered conductive glass (FTO, Pilkington Co., Ltd., 8 ohms/sq, 2.3-mm thick) was employed to prepare both the photo and counter electrodes. A dense, 100-nm-thick TiO_2 film as a blocking layer was prepared by spin coating a titanium(IV) bis(ethyl acetoacetato) diisopropoxide solution (2 wt% in butanol) at 1500 rpm for 10 sec, followed by calcination at 450 °C for 30 min. Viscous mixtures containing the PVC-g-POEM graft copolymer and preformed TiO_2 nanocrystals were deposited onto the FTO glass with a doctor-blade technique, followed by successive sintering at 450 °C for 30 min. The mesoporous TiO_2 films were sensitized overnight in a $Ru(dcbpy)_2(NCS)_2$ dye (dcbpy = 2,2-bipyridyl-4,4-dicarboxylato) solution (N719, 535-bisTBA, Solaronix, 13 mg, dissolved in 50 g distilled ethanol). Pt layered counter electrodes were prepared by spin-coating a 1 wt% H_2PtCl_6 solution in isopropanol onto the FTO glass and then sintering the film at 450 °C for 30 min. The I_2-free PEBII electrolyte solution in acetonitrile was directly cast onto the photoelectrode. First, a 2 wt% dilute PEBII solution was cast onto a dye-adsorbed TiO_2 photoanode and evaporated very slowly for easy penetration of the electrolytes through the nanopores of the TiO_2 layer. Next, a 10 wt% PEBII solution was cast onto the photoelectrode. Both electrodes were then superimposed and pressed between two glass plates to achieve slow evaporation of the solvent and a thin electrolyte layer. The cells were placed in a vacuum oven for one day for complete evaporation of the solvent.

The DSSCs were illuminated with a Keithley Model 2400 and a 1000 W xenon lamp (Oriel, 91193). The light intensity was homogeneous over an 8 × 8 in^2 area. A correction for the spectral mismatch between the simulated light and natural sunlight was made against a certified reference Si solar cell (Fraunhofer Institute for Solar Energy System, Mono-Si + KG filter, Certificate No. C-ISE269) for a sunlight intensity of one (100 mW/cm^2). This calibration was verified with an NREL-calibrated Si solar cell (PV Measurements Inc.). The DSSCs temperature was maintained at 25 °C throughout the measurement time using peltier cooling apparatus. The photoelectrochemical performances were calculated by the following equations:

$$FF = \frac{V_{max} J_{max}}{V_{oc} J_{sc}} \quad (1)$$

$$\eta(\%) = \frac{V_{max} J_{max}}{P_{in}} \times 100 = \frac{V_{oc} J_{sc} FF}{P_{in}} \times 100 \quad (2)$$

where J_{sc} is a short-circuit current density (mA/cm^2), V_{oc} is an open-circuit voltage (V), P_{in} is an incident light power, FF is the fill factor, η is an overall energy conversion efficiency and J_{max} (mA/cm^2) and V_{max} (V) are the current density and voltage in the *J*–*V* curve, respectively, at the point of maximum power output. The photoanodeactive area, determined by the aperture of a black mask, was 0.16 cm^2.

The IPCE was measured as a function of wavelength from 400 to 800 nm (K3100) under short circuit conditions using an irradiation of a 300 W xenon lamp, which was obtained by a series of light filters with different wavelengths. The IPCE value was calculated using the following equation:

$$IPCE = \frac{hcI}{\lambda P} \quad (3)$$

where *h* and *c* represent Planck's constant and the speed of light in a vacuum, respectively. *I* is the photocurrent density (mA/cm^2). λ and *P* are the wavelength (nm) and the intensity (mA/cm^2) of the incident monochromatic light, respectively.

Characterization: The surface and cross-sectional structures of TiO_2 photoanodes were characterized by field emission scanning electron microscopy (FE-SEM) (SUPRA 55VP, NICEM, Carl Zeiss). The specific surface area and specific pore volume of the TiO_2 films were measured from the N_2 adsorption-desorption isotherm via the Brunauer-Emmett-Teller (BET, for specific surface area) and Barrett-Joyner-Halenda (BJH, for specific pore volume) methods using a Belsorp-mini II device, after drying the sample at room temperature for one day in a vacuum oven. In advance of these measurements, the TiO_2 films were additionally degassed at 70 °C under dynamic vacuum (10^{-2} Torr) for 1 h. The diffuse reflectance spectra of TiO_2 photoanodes were acquired using a UV–visible spectrophotometer (Hewlett- Packard, Hayward, CF) over a sample area of roughly 5 × 5 μm^2 with a magnification of 100. A spectral range of 300–800 nm was explored using a tungsten-halogen lamp. Electrochemical impedance spectroscopy (EIS) analysis was used to investigate the internal resistance at the electrode/electrolyte interface and the recombination kinetics of TiO_2 photoelectrodes in DSSCs.

Measurement of Dye Adsorption: First, the N719 dye-sensitized TiO_2 photoanodes were dipped into 10.0 mL of a 10^{-2} M solution of NaOH in ethanol-H_2O (1:1). The mixture was stirred until complete desorption of the dye into the liquid occurred. The volume of the NaOH solution containing the fully desorbed dye was then measured by UV-visible spectroscopy. Amounts of the NaOH solutions were recorded, and the absorption value at 515 nm (as a function of wavelength) was used to

calculate the number of adsorbed N719 dye molecules according to the Beer-Lambert law, $A = \varepsilon lc$, where A is the absorbance of the UV-visible spectra at 515 nm, $\varepsilon = 14\ 100$/M cm is the molar extinction coefficient of the dye at 515 nm, l is the path length of the light beam, and c is the dye concentration.

Supporting Information

Supporting Information is available from the Wiley Online Library or from the author.

Acknowledgements

The authors acknowledge the financial support of the National Research Foundation (NRF) grant funded by the Korean government (MEST) through the Active Polymer Center for Pattern Integration (R11-2007-050-00000-0), the Pioneer Research Center Program (2008-05103) and the Korea Center for Artificial Photosynthesis (KCAP) (2012M1A2A2671781), and the Energy Efficiency & Resources of the Korea Institute of Energy Technology Evaluation and Planning (KETEP) grant funded by the Korea government Ministry of Knowledge Economy (20122010100040).

Received: December 27, 2012
Revised: February 5, 2013
Published online: March 27, 2013

[1] B. O'Regan, M. Gratzel, *Nature* **1991**, *353*, 737.
[2] a) S. Yanagida, Y. H. Yu, K. Manseki, *Acc. Chem. Res.* **2009**, *42*, 1827; b) K. Manseki, W. Jarernboon, Y. Youhai, K. J. Jiang, K. Suzuki, N. Masaki, Y. Kim, J. B. Xia, S. Yanagida, *Chem. Commun.* **2011**, *47*, 3120.
[3] S. Nejati, K. K. S. Lau, *Nano Lett.* **2011**, *11*, 419.
[4] C. Xu, J. Wu, U. V. Desai, D. Gao, *Nano Lett.* **2012**, *12*, 2420.
[5] W. S. Chi, J. K. Koh, S. H. Ahn, J. S. Shin, H. Ahn, D. Y. Ryu, J. H. Kim, *Electrochem. Commun.* **2011**, *13*, 1349.
[6] H. Cao-Cen, J. Zhao, L. Qiu, D. Xu, Q. Li, X. Chen, F. Yan, *J. Mater. Chem.* **2012**, *22*, 12842.
[7] Q. Li, J. Zhao, B. Sun, B. Lin, L. Qiu, Y. Zhang, X. Chen, J. Lu, F. Yan, *Adv. Mater.* **2012**, *24*, 945.
[8] a) C. P. Lee, P. Y. Chen, R. Vittal, K. C. Ho, *J. Mater. Chem.* **2010**, *20*, 2356; b) C. Y. Hsu, Y. C. Chen, R. Y. Y. Lin, K. C. Ho, J. T. Lin, *Phys. Chem. Chem. Phys.* **2012**, *14*, 14099.
[9] P. Docampo, S. Guldin, M. Stefik, P. Tiwana, M. C. Orilall, S. Huttner, H. Sai, U. Wiesner, U. Steiner, H. J. Snaith, *Adv. Funct. Mater.* **2010**, *20*, 1787.
[10] S. Guldin, S. Huettner, P. Tiwana, M. C. Orilall, B. Uelguet, M. Stefik, P. Docampo, M. Kolle, G. Divitini, C. Ducati, S. A. T. Redfern, H. J. Snaith, U. Wiesner, D. Eder, U. Steiner, *Energy Environ. Sci.* **2011**, *4*, 225.
[11] E. J. W. Crossland, M. Nedelcu, C. Ducati, S. Ludwigs, M. A. Hillmyer, U. Steiner, H. J. Snaith, *Nano Lett.* **2009**, *9*, 2813.
[12] K. J. Jiang, K. Manseki, Y. H. Yu, N. Masaki, K. Suzuki, Y. L. Song, S. Yanagida, *Adv. Funct. Mater.* **2009**, *19*, 2481.
[13] X. Z. Liu, W. Zhang, S. Uchida, L. P. Cai, B. Liu, S. Ramakrishna, *Adv. Mater.* **2010**, *22*, E150.
[14] J. K. Koh, J. Kim, B. Kim, J. H. Kim, E. Kim, *Adv. Mater.* **2011**, *23*, 1641.
[15] G. Q. Wang, L. A. Wang, S. P. Zhuo, S. B. Fang, Y. A. Lin, *Chem. Commun.* **2011**, *47*, 2700.
[16] a) S. H. Ahn, W. S. Chi, J. T. Park, J. K. Koh, D. K. Roh, J. H. Kim, *Adv. Mater.* **2012**, *24*, 519; b) S. H. Ahn, J. H. Koh, J. A. Seo, J. H. Kim, *Chem. Commun.* **2010**, *46*, 1935; c) D. Kyu Roh, J. T. Park, S. H. Ahn, H. Ahn, D. Y. Ryu, J. Hak Kim, *Electrochim. Acta* **2010**, *55*, 4976.
[17] a) Z. Lan, J. Wu, S. Hao, J. Lin, M. Huang, Y. Huang, *Energy Environ. Sci.* **2009**, *2*, 524; b) Q. Li, X. Chen, J. Zhao, L. Qiu, Y. Zhang, B. Sun, F. Yan, *J. Mater. Chem.* **2012**, *22*, 6674.
[18] I. Chung, B. Lee, J. He, R. P. H. Chang, M. G. Kanatzidis, *Nature* **2012**, *485*, 486.
[19] a) M. M. Lee, J. Teuscher, T. Miyasaka, T. N. Murakami, H. J. Snaith, *Science* **2012**, *338*, 643; b) H.-S. Kim, C.-R. Lee, J.-H. Im, K.-B. Lee, T. Moehl, A. Marchioro, S.-J. Moon, R. Humphry-Baker, J.-H. Yum, J. E. Moser, M. Gratzel, N.-G. Park, *Sci. Rep.* **2012**, *2*, 591.
[20] M. Zukalova, A. Zukal, L. Kavan, M. K. Nazeeruddin, P. Liska, M. Gratzel, *Nano Lett.* **2005**, *5*, 1789.
[21] a) E. S. Kwak, W. Lee, N. G. Park, J. Kim, H. Lee, *Adv. Funct. Mater.* **2009**, *19*, 1093; b) C. Y. Cho, J. H. Moon, *Adv. Mater.* **2011**, *23*, 2971; c) S.-H. Han, S. Lee, H. Shin, H. S. Jung, *Adv. Energy Mater.* **2011**, *1*, 546.
[22] a) S. Colodrero, A. Forneli, C. Lopez-Lopez, L. Pelleja, H. Miguez, E. Palomares, *Adv. Funct. Mater.* **2012**, *22*, 1303; b) N. Tetreault, M. Gratzel, *Energy Environ. Sci.* **2012**, *5*, 8506.
[23] F. Sauvage, D. H. Chen, P. Comte, F. Z. Huang, L. P. Heiniger, Y. B. Cheng, R. A. Caruso, M. Graetzel, *ACS Nano* **2010**, *4*, 4420.
[24] F. Z. Huang, D. H. Chen, X. L. Zhang, R. A. Caruso, Y. B. Cheng, *Adv. Funct. Mater.* **2010**, *20*, 1301.
[25] D. K. Roh, J. A. Seo, W. S. Chi, J. K. Koh, J. H. Kim, *J. Mater. Chem.* **2012**, *22*, 11079.
[26] N. Tetreault, M. Gratzel, *Energy Environ. Sci.* **2012**, *5*, 8506.
[27] a) S. Colodrero, A. Mihi, L. Haggman, M. Ocana, G. Boschloo, A. Hagfeldt, H. Miguez, *Adv. Mater.* **2009**, *21*, 764; b) S. Guldin, S. Huttner, M. Kolle, M. E. Welland, P. Muller-Buschbaum, R. H. Friend, U. Steiner, N. Tetreault, *Nano Lett.* **2010**, *10*, 2303.
[28] a) Q. Zhang, G. Cao, *J. Mater. Chem.* **2011**, *21*, 6769; b) J. Zhao, B. Sun, L. Qiu, H. Caocen, Q. Li, X. Chen, F. Yan, *J. Mater. Chem.* **2012**, *22*, 18380.
[29] J. Bicerano, *Prodiction of Polymer Properties*, Marcel Dekker, Inc., New York **1996**. Note that the solubility of parameter of POEM was calculated using the group contribution method.
[30] J. A. Riddick, W. B. Bunger, T. K. Sakano, *Organic Solvents: Physical Properties and Methods of Purfication*, John Wiley & Sons, Inc, New York **1986**.
[31] T. P. Chou, Q. F. Zhang, B. Russo, G. E. Fryxell, G. Z. Cao, *J. Phys. Chem. C* **2007**, *111*, 6296.